Journal of Catalysis 323 (2015) 132–144

Contents lists available at ScienceDirect

Journal of Catalysis

journal homepage: www.elsevier.com/locate/jcat

Glycerolysis of methyl oleate on MgO: Experimental and theoretical study of the reaction selectivity

P.G. Belelli [a,*], C.A. Ferretti [b], C.R. Apesteguía [b], R.M. Ferullo [c], J.I. Di Cosimo [b,*]

[a] Group of Materials and Catalytic Systems (GMSC) – IFISUR (UNS-CONICET), Av. Alem 1253, 8000 Bahía Blanca, Argentina
[b] Catalysis Science and Engineering Research Group (GICIC) – INCAPE (UNL-CONICET), Santiago del Estero 2654, 3000 Santa Fe, Argentina
[c] INQUISUR (UNS-CONICET), Av. Alem 1253, 8000 Bahía Blanca, Argentina

ARTICLE INFO

Article history:
Received 6 November 2014
Revised 2 January 2015
Accepted 3 January 2015

Keywords:
Glycerolysis
Monoglyceride
Isomer selectivity
DFT
Base catalysis
Molecular modeling
Periodic calculation

ABSTRACT

The liquid-phase MgO-promoted glycerolysis of methyl oleate, a fatty acid methyl ester (FAME), to give acylglycerol products was studied both, experimentally and by density functional theory (DFT). Catalytic results showed that strongly basic low coordination O^{2-} surface sites participate in kinetically relevant steps of the glycerolysis reaction. Changes in the selectivity toward the different mono- and diglyceride isomers were investigated by varying the reaction conditions. The main product was always α-glyceryl monooleate (α-MG), a monoglyceride with the ester fragment at one of the terminal positions of the glycerol molecule; the β-MG isomer, with the ester substituted at position 2 was obtained in much lower amounts.

The molecular modeling of glycerol (Gly) and FAME adsorptions as well as of the glycerolysis reaction was carried out using periodic DFT calculations and a model of stepped MgO surface. Results indicated that FAME was more weakly adsorbed than Gly; the latter adsorbs on a coordinatively unsaturated surface O^{2-} site with O—H bond breaking at position 2 of the Gly molecule, giving therefore a surface β-glyceroxide species. Calculations explained the apparent contradiction between the preferential formation of the α-MG isomer and the energetically favored dissociation of the secondary OH group of Gly that leads to the β-glyceroxide species. They predict that the β-glyceroxide species participates in the pathways conducting to both, α- and β-MG isomers. Synthesis of α-MG occurs by C—O coupling of β-glyceroxide with FAME at one of the two primary OH groups of the β-glyceroxide species. Two transition states (TS) and a tetrahedral intermediate (TI) are involved in both, α-MG and β-MG isomer formation. However, the pathway toward β-MG is limited by the large sterical effects associated to the TI formation. Contrarily, the TI leading to α-MG is relatively easy to form.

1. Introduction

During biodiesel synthesis by oil or fat transesterification, glycerol (Gly) is obtained as a coproduct representing 10% of the biodiesel production.

Lately, the increasing participation of biofuels in the energy matrix of many countries has generated a Gly surplus with the consequent drop of the unrefined Gly price. Thus, many efforts have been devoted recently to develop new applications intended to convert glycerol into value-added chemicals with the purpose to improve the economics of biodiesel production.

Gly is traditionally included in the formulation of food, cosmetic and pharmaceutical products, liquid detergents, and antifreeze [1]. Other recent applications comprise the production of hydrogen [2], liquid fuels [3], fuel additives [4], and chemicals [1,5,6]. Furthermore, environmental concerns are the driving force to replace a petroleum-based feedstock such as mineral Gly with its renewable biomass-derived substitute in the synthesis of new or conventional products.

Acylglycerols, the glycerol esters of fatty acids, can be synthesized by glycerolysis of fatty acid methyl esters (FAME) with Gly, as shown in Scheme 1. In particular, the monoesters or monoglycerides (MG) are an attractive option to transform bio-Gly into valuable chemicals; they are widely used as surfactants due to their emulsifying properties that help hydrophilic and lipophilic substances mix together. Therefore, they find application in many food, detergent, plasticizer, cosmetic, and pharmaceutical formulations [5,7].

* Corresponding authors. Fax: +54 291 4595142 (P.G. Belelli), +54 342 4511170 (J.I. Di Cosimo).
E-mail addresses: patricia.belelli@uns.edu.ar (P.G. Belelli), dicosimo@fiq.unl.edu.ar (J.I. Di Cosimo).

http://dx.doi.org/10.1016/j.jcat.2015.01.001
0021-9517/

Glycerolysis of FAME is a base-catalyzed transesterification reaction. In a previous work [8], the glycerolysis reaction was studied using methyl oleate (C18:1) as FAME and MgO as catalyst. We investigated the chemical nature of the base sites responsible for the catalytic activity of MgO, both experimentally and by density functional theory (DFT). The catalytic results showed the preferential formation of α-MG, Scheme 1, indicating that the FAME-Gly coupling with formation of a new C—O bond is produced mostly at the primary hydroxyl of the glycerol molecule after O—H bond breaking. Contrarily, the DFT calculations using the cluster model approximation [8] predicted that upon Gly adsorption on MgO, the O—H bond of the secondary hydroxyl is dissociated, forming a surface β-glyceroxide, Scheme 2, that might give rise to a reaction pathway leading β-MG.

To get insight into this selectivity issue, in this work, we continue our studies of the methyl oleate glycerolysis on MgO. We report our investigations about the effect of different operational variables on the glyceride isomer selectivity. Furthermore, molecular modeling using periodic calculations supports the preferential formation of α-MG and allows us to postulate reaction mechanisms for α-MG and β-MG formation. The reasons for the former contradictory results are therefore elucidated since calculations show that the β-glyceroxide surface species participates in the formation of both MG isomers.

2. Experimental and computational methods

2.1. Catalyst preparation and characterization

Magnesium oxide catalyst was prepared by hydration with distilled water of commercial MgO (Carlo Erba 99%; 27 m^2/g). Details are given elsewhere [9]. The resulting $Mg(OH)_2$ was decomposed in a N_2 flow for 18 h at 773 K to obtain high-surface area MgO. The sample was finally ground and sieved, and the particles with average particle size of 177–550 μm were used in the catalytic experiments.

The BET surface area (*SA*) was determined by N_2 physisorption at 77 K in a NOVA-1000 Quantachrome sorptometer. The structural properties of MgO were determined by X-ray diffraction (XRD) using a Shimadzu XD-D1 diffractometer equipped with Cu Kα radiation source (λ = 0.1542 nm).

MgO base properties were measured by temperature programmed desorption (TPD) and infrared spectroscopy (FTIR) of CO_2. For the TPD experiment, the sample was pretreated in situ in a N_2 flow at 773 K to remove water and carbonates formed during storage, cooled down to room temperature, and then exposed to a flowing mixture of 3% of CO_2 in N_2, until surface saturation was achieved (5 min). Weakly adsorbed CO_2 was removed by flushing with N_2. Finally, the temperature was increased to 773 K at a ramp rate of 10 K/min. Desorbed CO_2 was converted in CH_4 on a methanation catalyst (Ni/Kieselguhr) and then analyzed using a flame ionization detector (FID). Total base site number (N_b, μmol/g) was measured as the evolved CO_2 obtained by integration of TPD curves. The total base site density in μmol/m^2 was calculated as $n_b = N_b/SA$.

The chemical nature of adsorbed surface CO_2 species was determined by FTIR after CO_2 adsorption at room temperature and sequential evacuation at increasing temperatures. The sample was pressed in a wafer and degassed in vacuum at 773 K for 1 h and then cooled down to room temperature. The spectrum of the pretreated catalyst was then taken. After admission of 5 kPa of CO_2 and evacuation at 298, 373, 473, and 573 K, the CO_2 adsorption spectra were recorded at room temperature. Spectra of the adsorbed species were obtained by subtracting the catalyst spectrum. Data were collected in a Shimadzu FTIR Prestige-21 spec-

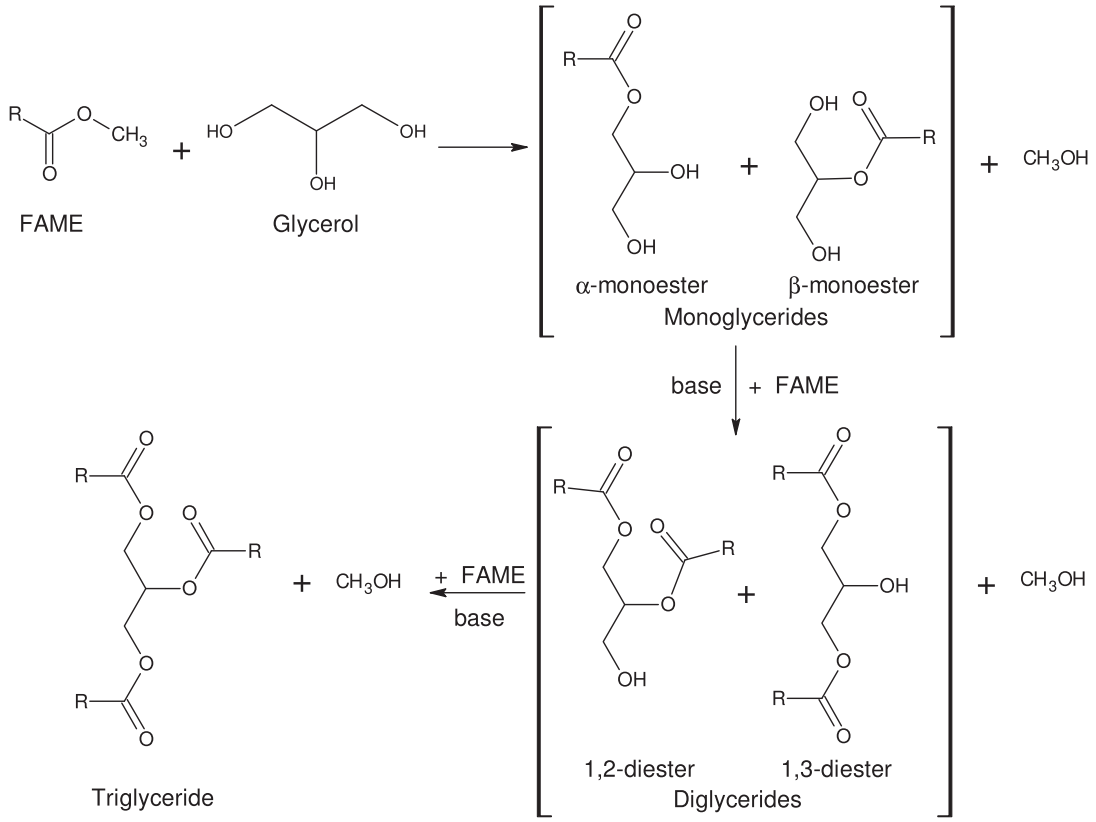

Scheme 1. Monoglyceride (MG) synthesis by glycerolysis of FAME and consecutive reactions to diglycerides (DG) and triglyceride (TG).

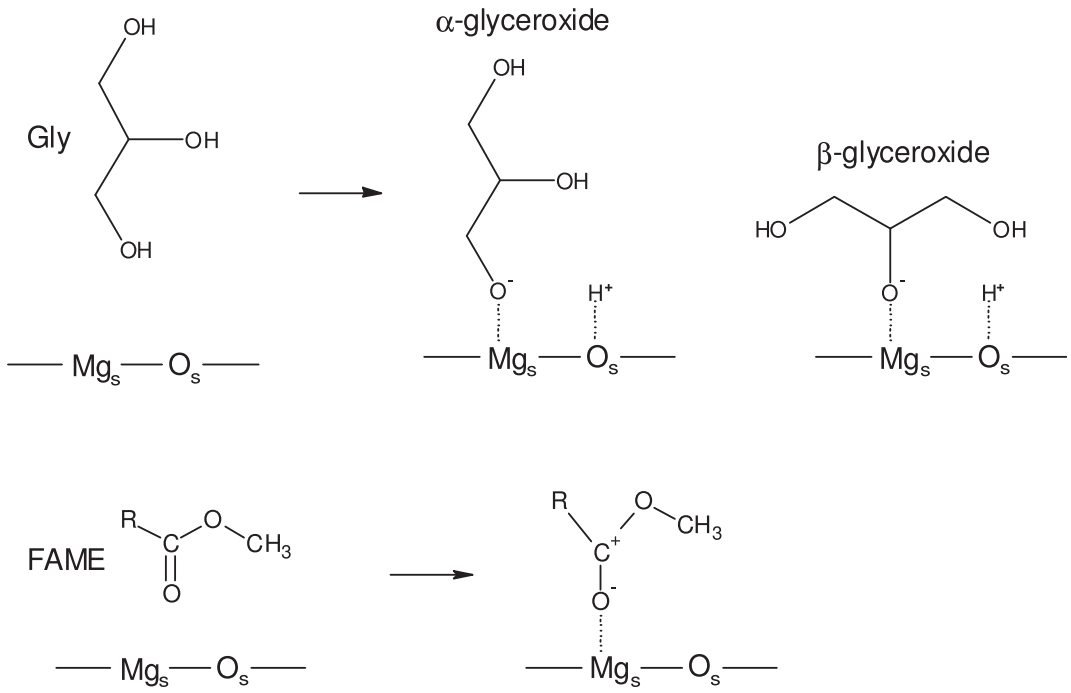

Scheme 2. Formation of surface glyceroxide species from glycerol and FAME surface activation on MgO.

trometer using an inverted T-shaped cell fitted with CaF_2 windows that contains the sample pellet. The absorbance scale was normalized to 20 mg.

2.2. Catalytic tests

The glycerolysis of a fatty acid methyl ester (methyl oleate, Fluka, >60.0%, with 86% total C18 + C16 esters as determined by gas chromatography) with glycerol (Aldrich, 99.0%) was carried out at 483–503 K in a seven-necked cylindrical glass reactor with mechanical stirring equipped with a condenser to remove the methanol generated during reaction. The 4-phase reactor was operated in a batch regime for the liquid and solid phases at atmospheric pressure. A continuous flow of N_2 (35 ml/min) was used to remove the methanol produced out of the reactor. More details are given elsewhere [10]. Gly/FAME molar ratios of 2–6 and a catalyst/FAME ratio (W_{cat}/n^0_{FAME}) of 8 g/mol were used. Catalyst was pretreated ex situ at 773 K for 6 h to remove adsorbed water and carbon dioxide and kept overnight at 373 K in flowing N_2 until use and then quickly transferred to the reactor without exposing it to air to start the reaction. The reactor was assumed to be perfectly mixed. Eleven samples of the reaction mixture were extracted and analyzed during the 8-h catalytic run.

Reaction products were α- and β-glyceryl monooleates (monoglycerides, MG), 1,2- and 1,3-glyceryl dioleates (diglycerides, DG), and glyceryl trioleate (triglyceride, TG). Samples were silylated to improve compound detectability. Details on the analytical procedures are given elsewhere [11]. Silylated samples were analyzed by GC in a SRI 8610C gas chromatograph equipped with a flame ionization detector (FID), on-column injector port, and a HP-1 Agilent Technologies 15 m × 0.32 mm × 0.1 μm capillary column. Quantification was carried out using authentic standards of glyceryl trioleate (Sigma, 65.0%) and a commercial mixture of glyceryl mono- and dioleate of known composition (Fluka, 71.5% MG and 25.3% DG).

Conversion (X_{FAME}, referred to the total content of esters in the reactant), selectivity (S), and yield (Y) were calculated through the following equations (n_j, mol of product j; MG, monoglycerides (both isomers); DG, diglycerides (both isomers); TG, triglyceride):

$$X_{FAME}\ (\%) = \frac{n_{MG} + 2n_{DG} + 3n_{TG}}{n_{MG} + 2n_{DG} + 3n_{TG} + n_{FAME}} \cdot 100$$

$$S_{MG}\ (\%) = \frac{n_{MG}}{n_{MG} + 2n_{DG} + 3n_{TG}} \cdot 100$$

$$S_{DG}\ (\%) = \frac{2n_{DG}}{n_{MG} + 2n_{DG} + 3n_{TG}} \cdot 100$$

$$S_{TG}\ (\%) = \frac{3n_{TG}}{n_{MG} + 2n_{DG} + 3n_{TG}} \cdot 100$$

$$Y_j\ (\%) = X_{FAME} \cdot S_j \cdot 100$$

2.3. Computational details and models

The Vienna Ab-initio Simulation Package (VASP) [12–14] was used to perform all the periodic calculations reported in this work. The Kohn–Sham equation was solved using a plane wave basis set. A good convergence was achieved with a cutoff energy of 350 eV for the kinetic energy. The projector augmented wave (PAW) method developed by Blöch [15] was used to describe the core electron effect in the electronic density of the valence electrons [16]. PAW is a frozen core method which considers the exact shape of the valence wave functions instead of pseudo-wave functions. The exchange and correlation effects were described by the generalized gradient approximation (GGA) using the functional expressed by Perdew, Burke and Ernzerhof (PBE) [17]. The two-dimensional Brillouin integrations in the reciprocal space were performed on a grid of 3 × 2 × 1 Monkhorst–Pack special k-points [18]. The Methfessel–Paxton method with a smearing width of σ = 0.2 eV was applied, and the reported total energies were then extrapolated to $\sigma \rightarrow 0$ eV [19].

A slab representing a monoatomic step on the MgO (100) surface was constructed following the MgO (510) plane. The resulting

supercell contains 90 atoms distributed in three layers. We have observed that the addition of a forth layer produces a negligible variation of the superficial energy. The cell is sufficiently large to avoid lateral interaction between adsorbed molecules. The vacuum region between neighboring slabs in the perpendicular direction to the surface was set to ~15 Å, corresponding to seven ideal bulk layers. The gas-phase geometries of isolated Gly and FAME were completely optimized using a 20 × 20 × 20 supercell. Periodic calculations indicate that the (100) surfaces of alkaline-earth oxides present very slight relaxation [20,21]. For this reason, only the atoms corresponding to the first layer were allowed to relax while all the adsorbed molecules were completely optimized. The relaxation of atoms placed at the edge of stepped MgO produces the angle increase from 90° (unrelaxed surface) to 101.6° and 104.0° for $O_{4C}Mg_{6C}O_{5C}$ and $Mg_{4C}O_{6C}Mg_{5C}$ angles, respectively, in good agreement with the results of Chizallet et al. [22].

The adsorption energy (E_{ads}) of Gly or FAME was evaluated according to the following total energy difference: $E_{ads} = E_{(molecule-MgO)} - E_{(MgO)} - E_{(molecule(g))}$, where "molecule" is either Gly or FAME. We also define the reaction energy (E_{reac}) as the relative energy with respect to the Gly + FAME + MgO as isolated species. In all the cases, negative values indicate exothermic processes.

Complementary calculations including solvation effects were performed; the results are presented at the end of Section 3.4.3. Three FAME molecules were added to mimic the solvent. Two of these molecules were located above the adsorbed Gly and FAME species and the third one interacting with the β-GlyOx–FAME contact.

3. Results and discussion

3.1. Characterization of MgO

The hydration of commercial MgO and subsequent decomposition of the resulting $Mg(OH)_2$ followed by stabilization at 773 K gave rise to a MgO catalyst with an increased BET surface area (*SA*) of 189 m^2/g. This is attributed to the development of a porous structure caused by the gaseous evolution during $Mg(OH)_2$ decomposition [23]. Also, the final MgO catalyst presents a pore volume of 0.38 ml/g and a mean pore diameter of about 80 Å. The X-ray diffractogram of the calcined material (not shown here) confirmed the presence of only a MgO periclase phase (ASTM 4-0829).

The surface base properties of MgO were investigated by combination of TPD and IR measurements the CO_2 preadsorbed at room temperature. The total base site number, N_b (μmol/g), calculated by integration of TPD profile (not shown) was 655 μmol/g.

On a perfect MgO (100) surface, Mg^{2+} and O^{2-} are five-coordinated ions (Mg_{5c} and O_{5c}), but on the surface of the high-surface area MgO catalyst used here, both ions are also present with coordination numbers (*L*) lower than 5 depending on the location in corners or edges, so that *L* is 5, 4 or 3 for ions in terrace, edge or corner sites, respectively, as sketched in Fig. 1.

In a previous work [24], we used FTIR of CO_2 preadsorbed at room temperature to study the chemical nature of surface oxygen species on similar high-surface area MgO catalyst. By this technique, several CO_2 adsorbed species formed on different surface oxygen-containing species or on oxygen anions with different coordination numbers could be detected. We identified at least three different CO_2 adsorption species: unidentate and bidentate carbonates, and bicarbonate. Unidentate carbonate (U.C.) formation requires coordinatively unsaturated oxygen anions, such as those present in corners or edges (O_{3c} or O_{4c}) and exhibits a symmetric O—C—O stretching at 1360–1400 cm^{-1} and an asymmetric O—C—O stretching at 1510–1560 cm^{-1}. Bidentate carbonate (B.C.) forms on metal–oxygen acid–base sites such as Mg_{5c}—O_{5c} pairs, which are predominant on the terrace sites of MgO. This species shows a symmetric O—C—O stretching at 1320–1340 cm^{-1} and an asymmetric O—C—O stretching at 1610–650 cm^{-1}. Bicarbonate (Bic) species formation involves surface hydroxyl groups and shows a C—OH bending mode at 1220 cm^{-1} as well as symmetric and asymmetric O—C—O stretching bands at 1480 cm^{-1} and 1650 cm^{-1}, respectively [25,26].

The FTIR analysis of CO_2 adsorbed at room temperature and evacuated at 298, 373, 473, and 573 K was carried out on MgO. Fig. 2 shows the spectra obtained in the 1900–1100 cm^{-1} carbonate region. The overlapping broad infrared bands confirmed the presence of different carbonate species, i.e., base sites of different nature formed on the non-uniform surface of MgO, as explained above (Fig. 1). Bic species disappeared after evacuation at 373 K revealing the weak basic features of the surface OH groups of MgO. In contrast, U.C. and B.C. species remained on the surface even after evacuation at 573 K; U.C. species were more resistant to evacuation at high temperatures. Thus, results in Fig. 2 suggest the formation of weak, medium, and strong surface oxygen species on MgO, with the following base strength order: low coordination O^{2-} anions > oxygen in Mg^{2+}—O^{2-} pairs > OH groups.

Quantification of the contribution of these oxygen species was carried out by deconvolution of the TPD profile (not shown here) in three desorption bands, reaching maximum desorption rates at about 400, 450, and 550 K. The total base site density (n_b) was 3.47 μmol/m^2, and the contribution of each peak, identified as the density of weak (n_{OH}), medium (n_{Mg-O}), and strong (n_O) base sites, was 0.55 μmol/m^2, 1.26 μmol/m^2, and 1.66 μmol/m^2, respectively. Thus, the MgO surface contains mainly medium and strong base sites. In a recent paper [8], we demonstrated that the density of weak, medium, and strong base sites dramatically depends on the MgO activation procedure. An increase of the calcination temperature generates smother MgO surfaces that resemble the steps of the surface depicted in Fig. 1. Thus, surface defects such as low coordination oxygen atoms located in corners or edges disappeared upon treatment at high temperatures causing a decrease of n_O. As a consequence, the total base site density and the overall basicity of a MgO sample calcined at high temperatures (873 K) are lower than those of a sample treated at 673 K.

3.2. The glycerolysis reaction. MgO active site for monoglyceride synthesis

MgO was tested in the glycerolysis of FAME in a reactor consisting of four phases: the solid catalyst; the bottom liquid layer formed by the Gly phase; the top liquid fatty phase containing FAME and glyceride products; and the gas phase containing methanol that is continuously removed from the reactor. FAME is not soluble in Gly and Gly is slightly soluble in the FAME phase, and therefore, the reaction occurs in the upper phase where both reactants coexist. More details of the glycerolysis reaction are given elsewhere [10].

Fig. 3 shows a catalytic experiment carried out with MgO at typical reaction conditions (493 K). Results presented in Fig. 3 are the FAME conversion (X_{FAME}) and yield of the different glycerides (Y_j, *j* = α-MG, β-MG, 1,2-DG, and 1,3-DG). MgO converts FAME at high rates, reaching ~95% conversion at the end of the 8 h-run. The predominant formation of monoglycerides can be observed, with α-MG being the main isomer ($Y_{\alpha\text{-MG}}$ = 53%) over β-MG. Diglycerides appeared mainly as 1,3-DG and to a lesser extent as 1,2-DG. No TG formation was detected at any reaction condition on MgO.

The non-zero initial slope (slope at $t = 0$) of the $Y_{\beta\text{-MG}}$ vs. time curve (open triangles in Fig. 3) suggests that β-MG is a primary product of the glycerolysis reaction formed catalytically and directly from FAME and not consecutively from α-MG. On the con-

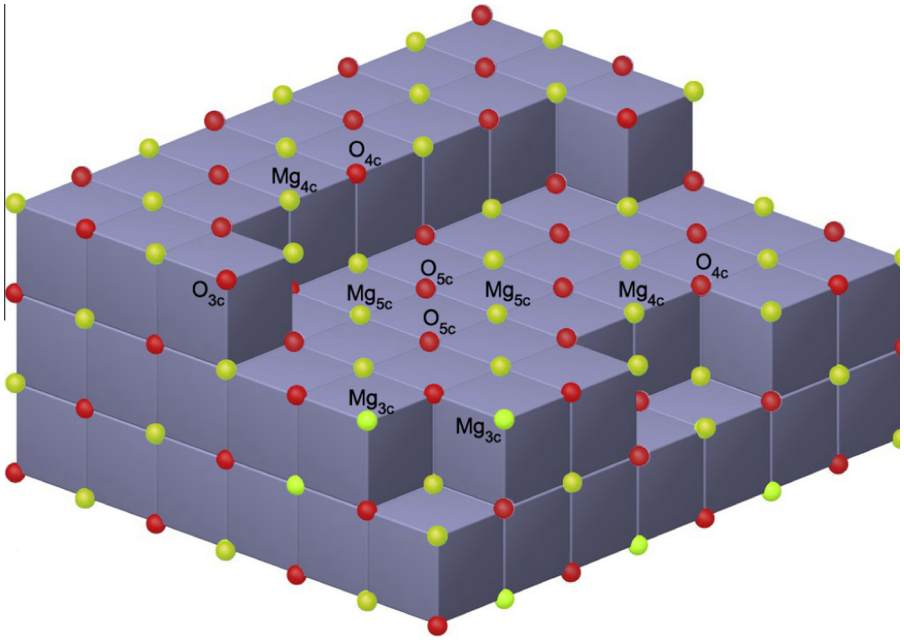

Fig. 1. Scheme of a stepped MgO (1 0 0) surface with O_{Lc} and Mg_{Lc} ions in different positions (L: coordination number). Terrace sites: O_{5c}, Mg_{5c}; edge sites: O_{4c}, Mg_{4c}; corner sites: O_{3c}, Mg_{3c}.

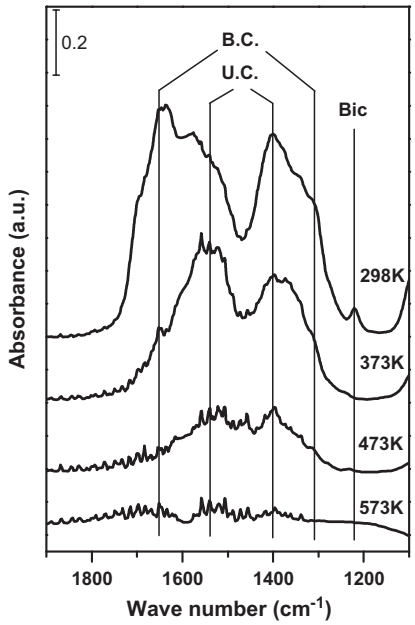

Fig. 2. FTIR spectra of CO_2 adsorbed at room temperature on MgO and desorbed at increasing evacuation temperatures [MgO calcined at 773 K; B.C.: bidentate carbonate; U.C.: unidentate carbonate; Bic: bicarbonate].

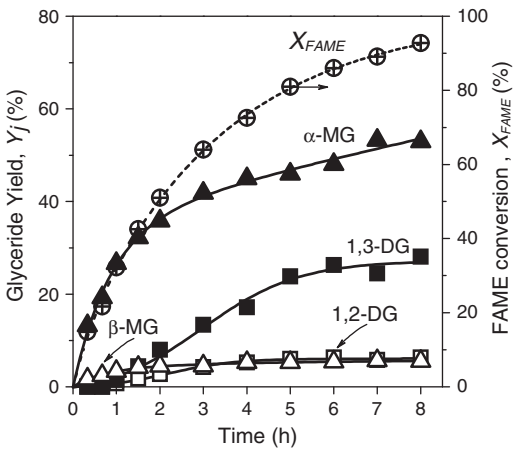

Fig. 3. FAME conversion and glyceride yields [MgO calcined at 773 K, Gly/FAME = 6.0, T = 493 K].

trary, the zero initial slope of the $Y_{1,2\text{-DG}}$ and $Y_{1,3\text{-DG}}$ curves indicates consecutive formation from α- and β-MG as postulated in Scheme 1. However, isomer interconversion at higher reaction times cannot be ruled out, neither the existence of disproportionation reactions [10].

In previous papers [8,23], we investigated the chemical nature of the MgO base sites involved in the glycerolysis reaction. We found a decline of the catalytic activity measured on MgO samples calcined at increasing temperatures, following a trend similar to that observed for the strong base site density (n_O), as explained in Section 3.1. In fact, the linear correlation between the initial MG formation rate and n_O presented in Fig. 4 suggests that the reaction rate-determining step involves the participation of strong base sites. Thus, monoglyceride synthesis by glycerolysis of methyl oleate is mainly promoted by coordinatively unsaturated oxygen anions present in corners or edges of the non-uniform surface of MgO.

3.3. Effect of the experimental conditions on the selectivity toward glycerides

We have studied in the past that diffusional limitations can be neglected at the experimental conditions used in the present work (small particle size and high stirring rate). Besides, as most transesterification reactions, the glycerolysis of Gly with methyl oleate toward glyceryl monooleate and methanol, Scheme 1, is thermoneutral [10]. Thus, in a kinetically controlled reaction system, a change in the reaction temperature would affect mainly the overall kinetic rate constant, as predicted by the Arrhenius equation, but

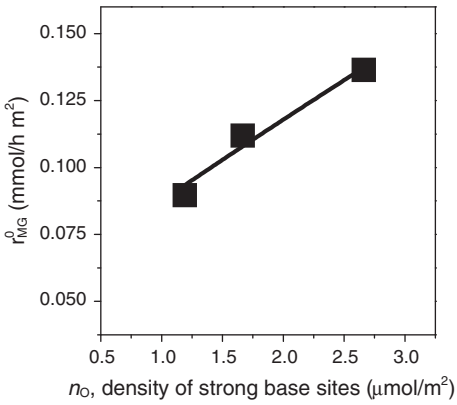

Fig. 4. Initial MG formation rate as a function of the density of strong base sites [MgO calcined at 673, 773, and 873 K, Gly/FAME = 4.5, T = 493 K].

also the Gly solubility in the fatty phase. Therefore, the reaction will proceed faster as Gly solubility in the fatty phase increases, which occurs at increasing temperatures [27,28]. Measurements of the Gly solubility in the FAME phase showed indeed a Gly concentration of just 1.15 wt.% at 493 K which slightly increases to 1.65 wt.% at 523 K. Therefore, we anticipate a positive effect of the reaction temperature increase on the reaction rate in the FAME phase. However, the effect on the selectivity is less evident and formation of other competing products is likely to occur at high temperatures, such as the undesirable formation of polyglycerols above 533 K [29].

At the typical reaction conditions of Fig. 3, α-MG is the main product but in order to investigate the effect of the reaction temperature on the selectivity, catalytic tests were performed on MgO at 483, 493, and 503 K using a Gly/FAME ratio of 4.5. As expected, FAME conversion increased with the reaction temperature reaching 80% at 483 K, 90% at 493 K, and 96% at 503 K after 8 h of reaction. Fig. 5 shows the product distribution in terms of selectivity as a function of the reaction temperature at two X_{FAME} levels. MG and in particular the α-MG isomer predominate at 483–503 K. The selectivity to the α-MG isomer is enhanced by increasing the reaction temperature at the expense of diglycerides, whereas selectivity to β-MG remains unchanged. Thus, the increase of the reaction temperature from 483 to 503 K remarkably affects the S_{MG}/S_{DG} ratio. For instance, at X_{FAME} = 35%, Fig. 5a, the ratio increases from 4.5 to 17.9. Similar results are observed at a conversion level of 50%, Fig. 5b. The enhancement of the S_{MG}/S_{DG} ratio upon a temperature increase is consistent with a higher activation energy of the MG synthesis step compared to that of DG, Scheme 1 [30]. In fact, we have previously calculated values of 26 and 19 kcal/mol for MG and DG formation, respectively, on MgO catalysts with similar basic properties as the one used here [10]. The effect of temperature is also noticeable on the distribution of DG, showing a higher contribution of the 1,3-DG isomer at lower temperatures.

According to Scheme 1, the stoichiometry of the MG synthesis requires a Gly/FAME molar ratio of 1:1. However, a glycerol excess is often used to drive the reaction forward and to reach high FAME conversions. In fact, we have shown that using a Gly/FAME = 1 at 493 K, the MGs formed in the early stages of the reaction are readily converted to DGs [31]. This is explained by total Gly consumption in the reaction zone (the FAME phase) which favored the consecutive reaction of MG with FAME over the glycerolysis of FAME with Gly, as sketched in Scheme 1. Furthermore, the Gly solubility in the FAME phase measured at 493 K increased from 0.86 wt.% at Gly/FAME = 1 to 1.15 wt.% at Gly/FAME = 4.5. Thus, Gly/FAME ratios >1 are expected to favor the selective formation of MG. However, the effect of the glycerol excess on the catalytic performance can be hardly predicted because glycerol is more hydrophilic than FAME and might adsorb strongly on the MgO surface, thereby blocking the active sites.

Here, we are reporting the effect of varying the Gly/FAME ratio at 493 K. The 8 h-tests were carried out at a constant W_{cat}/n^0_{FAME} ratio and changing the molar amount of Gly in order to obtain Gly/FAME molar ratios in the range of 2–6. The X_{FAME} at the end of the run increased with Gly/FAME so that values of 78%, 85%, 90%, and 93% were measured for Gly/FAME ratios of 2, 3, 4.5, and 6, respectively. These results confirm that high Gly/FAME ratios increase the availability of Gly to react with FAME in the reaction zone.

The selectivity to glycerides as a function of the Gly/FAME ratio at 35% and 50% FAME conversion is shown in Fig. 6a and b, respectively. Results suggest a negligible effect of the reactant ratio on the glyceride distribution, with α-MG being always the main product. Similarly, a S_{MG}/S_{DG} ratio of ~13 was rather independent of the Gly/FAME ratio at 35% conversion, Fig. 6a. However, at 50% conversion, the S_{MG}/S_{DG} ratio dropped to a constant value of ~6 as a consequence of the increasing selectivity to DG at higher conversions.

In conclusion, results of Figs. 5 and 6 indicate that the reaction temperature has a more marked influence on the selectivity than the reactant ratio. Furthermore, α-MG is always the main reaction product in the wide range of experimental conditions, reaching selectivities of up to 85%.

3.4. Theoretical studies of the kinetics of FAME glycerolysis on MgO

As explained above, the linear correlation between the catalytic activity and n_O of Fig. 4 clearly suggests that on MgO, the glycerol-

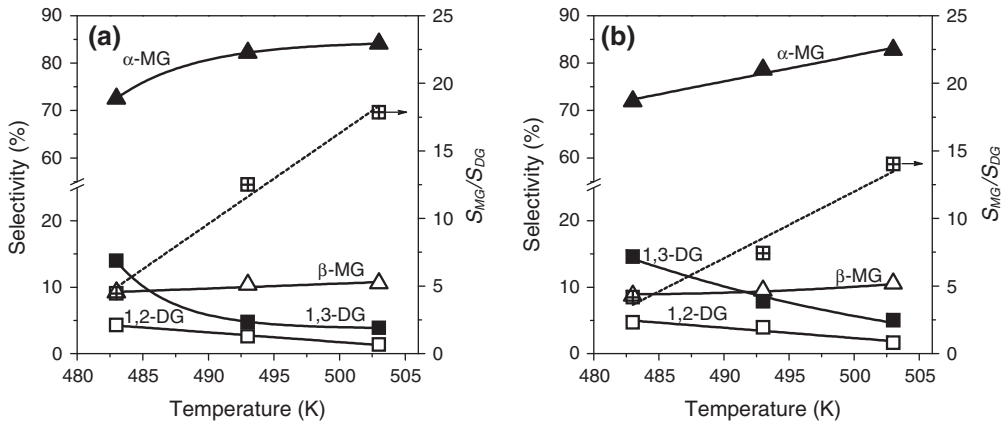

Fig. 5. Effect of the reaction temperature on glyceride selectivity and on S_{MG}/S_{DG} selectivity ratio at FAME isoconversion. (a) X_{FAME} = 35%; (b) X_{FAME} = 50% [Gly/FAME = 4.5].

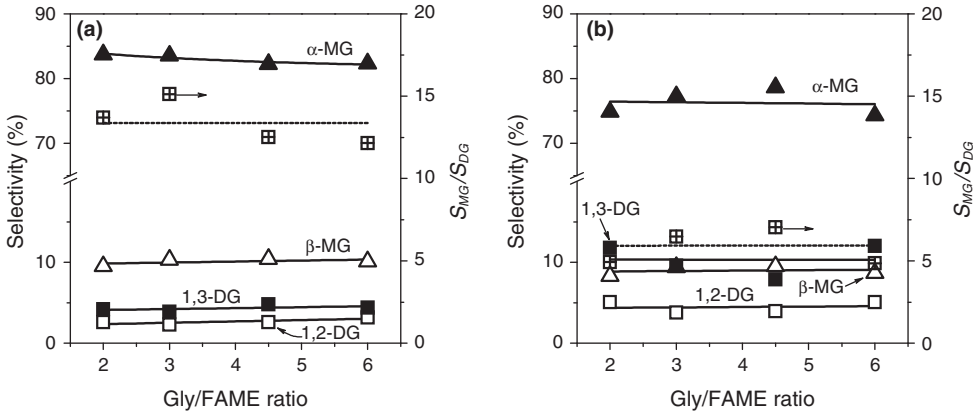

Fig. 6. Effect of the Gly/FAME ratio on glyceride selectivity and on S_{MG}/S_{DG} selectivity ratio at different FAME isoconversion. (a) X_{FAME} = 35%; (b) X_{FAME} = 50% [T = 493 K].

ysis reaction mostly occurs on strong base sites such as low coordination O^{2-} anions. The role of these surface species is expected to be the O—H bond dissociation of the hydroxyl groups present in the Gly molecule with formation of a surface glyceroxide and a proton, as depicted in Scheme 2, for primary (α-glyceroxide) and secondary (β-glyceroxide) hydroxyls. Gly contains three hydroxyl groups, and therefore, the Gly dissociative adsorption can take place in theory, with the O—H bond breaking at one, two, or the three OH groups.

On the other hand, as in many base-catalyzed reactions, surface Lewis acid sites, i.e., the Mg^{2+} cations, participate in the stabilization of negatively charged reaction intermediates (the glyceroxide anion). Another possible role of the Mg^{2+} cations is the activation of the FAME molecule and polarization of its C=O bond, as sketched in Scheme 2, so that to facilitate the attack of the glyceroxide anion to the positively charged carbonyl carbon of FAME.

The synthesis of MG and DG requires the formation of a new C—O bond between FAME and Gly after cleavage of the O—H bonds of Gly. Figs. 3, 5 and 6 show that the main product of the glycerolysis of methyl oleate was always the α-glyceryl monooleate (α-MG), followed by the 1,3 isomer of glyceryl dioleate (1,3-DG) in a wide range of experimental conditions. Clearly, the primary OH groups of Gly were involved in the formation of those products by the reaction sequence of Scheme 1. Time ago, we studied the reduction of ketones by hydrogen transfer reactions on MgO using alcohols as a hydrogen source and found that aliphatic secondary alcohols were better hydrogen donors than the primary ones [32]. Similar findings were reported by other authors [33]. An explanation for this outcome is that secondary alcohols have better reducing capacities than primary alcohols because the corresponding dialkyl ketones present higher reduction potentials than aldehydes [34,35]. Based on that, now, we would have expected the secondary O—H bond of Gly to be preferentially activated giving β-MG, and probably 1,2-DG, as the main products.

The preferential formation of α-MG and 1,3-DG compared to β-MG and 1,2-DG is possibly a consequence of the higher accessibility and number of primary OH groups in the Gly molecule or may be due to steric hindrance for C—O coupling at the secondary OH group. Consequently, the search for a suitable and supported explanation for this behavior is the motivation for the theoretical calculations of the following sections.

To elucidate the selectivity issue, we carried out calculations within the density functional theory (DFT) formalism using the Gaussian-03 package [8] and the cluster model approximation. The molecular modeling of the Gly and FAME adsorptions on a MgO (100) surface was performed using four different clusters. Thus, the surface of the high-surface area MgO catalyst was represented as containing four different adsorption sites (Fig. 1): the terrace site with Mg_{5c}—O_{5c} pairs (L = 5) that corresponds to medium strength base sites; the edge and the O-apical corner sites modeling the strongly basic O_{4c} (L = 4) and O_{3c} (L = 3) sites, respectively, and a Mg-apical corner (Mg_{3c}; L = 3) that models a Lewis acid site. In agreement with the catalytic results, the molecular modeling of Gly adsorption on those four different cluster sites predicted that dissociative chemisorption of the O—H bond occurs only on strong base sites (edge sites) whereas non-dissociative adsorption takes place on medium strength base sites such as those of terrace sites. The calculations also showed that none of the primary OH bonds dissociates in a barrierless fashion on either the MgO terrace or edge sites and that the strong Gly-edge site interaction caused the dissociative adsorption at the secondary OH group. Thus, due to O—H bond breaking, two new surface species were formed: a hydroxyl group between the abstracted H and a surface oxygen, O_s, and a β-glyceroxide stabilized on a surface cation, Mg_s (Scheme 2). Consequently, these previous calculations do not provide an answer for the experimental results showing the preferential formation of α-MG.

Although those previous calculations with cluster models allowed us to evaluate comparatively the Gly and FAME adsorptions, they present limitations mainly due to the large number of atoms involved. Besides, these models show the so-called "edge effects" because the surfaces are modeled by a finite number of atoms. Extended surfaces are better represented by periodic calculations. That is why in the present work, we have widen our studies using the VASP package to predict the energetic profile of the glycerolysis reaction and to calculate kinetic parameters in order to elucidate the predominant formation of α-MG.

3.4.1. Adsorption of Gly and FAME on MgO

Fig. 7 shows different views of the slab used to model the stepped MgO surface.

Firstly, Gly and FAME adsorption processes were modeled independently. For the Gly adsorption modeling, different geometrical modes were tested and five geometries with diverse interactions between Gly and the MgO surface were obtained. Optimized geometrical structures for Gly adsorption on the stepped MgO surface are shown in Fig. 8, and the results are summarized in Table 1. The different configurations are labeled as nOH(m), where n and m represent the amount and position of the OH groups interacting with the surface, respectively. Thus, m is 1 or 3 for primary hydroxyls and 2 for the secondary one. In order to compare with the distances reported in Table 1, the geometry for the isolated Gly molecule was also calculated; the obtained intramolecular distances resulted to

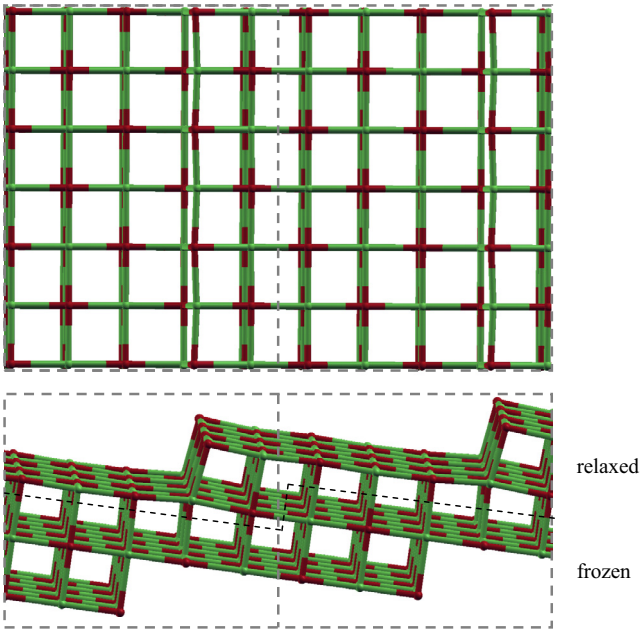

Fig. 7. Top view (top) and side view (bottom) of the slab used as model for the stepped MgO surface. Red and green balls correspond to O and Mg atoms, respectively. (For the interpretation of the references to color in this figure legend, the reader is referred to the Web version of this article.)

be the following: $d_{(C-C)} \approx 1.52$ Å, $d_{(C-O)} \approx 1.44$ Å, $d_{(C-H)} \approx 0.98$ Å, and $d_{(O-H)} \approx 1.09$ Å.

In all the cases, Gly interacts preferentially with Mg_s and O_s ions at the edge of the stepped MgO surface. Dissociative adsorption modes present a stronger interaction with the surface than non-dissociative adsorption modes. In agreement with previous results obtained using the cluster model approximation [8], the present calculations predict no spontaneous dissociative adsorption modes involving the primary O—H groups. The weakest interaction with the surface corresponds to the non-dissociative adsorption indicated as $3OH_a$ (Fig. 8d). In this configuration, both primary hydroxyl groups form hydrogen bonds with the strongly basic O^{2-}_{4c} sites, and the secondary one interacts with a terrace O^{2-}_{5c} ion with a longer hydrogen bond. In the non-dissociative adsorption 2OH(2,3) (Fig. 8c), the secondary OH group has a short hydrogen bond (1.43 Å) with the O—H distance longer than in free glycerol (1.09 Å). In this case, its E_{ads} indicates a stronger interaction than $3OH_a$.

In the other three geometries, Gly interacts dissociatively by breaking the O—H bond of the secondary hydroxyl group. As a result, a surface OH at the edge is formed together with the β-glyceroxide species (β-GlyOx) which strongly interacts with Mg^{2+}_{4c}. Besides, the adsorption becomes more stable as the number of primary hydroxyl groups interacting with the surface increases through the formation of hydrogen bonds. Indeed, the 1OH(2) geometry does not have hydrogen bonds (Fig. 8a), 2OH(1,2) has only one (Fig. 8b), and in the most stable geometry, $3OH_b$, both primary OH groups are linked with the surface (Fig. 8e). Besides, in all the cases, an additional hydrogen bond is formed between the O and H atoms formerly belonging to the secondary hydroxyl. This interaction contributes to the high stability of the glyceroxide species. As it was previously reported [8], the O—H bond dissociation is a required condition in the reaction mechanism and it is more probably to take place on low coordination O^{2-} sites, in particular at edge O^{2-}_{4c} sites.

From these results, we can observe that as the $d_{(O-H)}$ increases (and at the same time the $d_{(H-Os)}$ and $d_{(O-Mgs)}$ decrease), the magnitude of E_{ads} increases, Table 1. This trend indicates that Gly can easily dissociate on steps of MgO to form the β-GlyOx species. In the past, the interaction of Gly and related molecules was theoretically studied on monoatomic steps of CaO. Contrary to our results

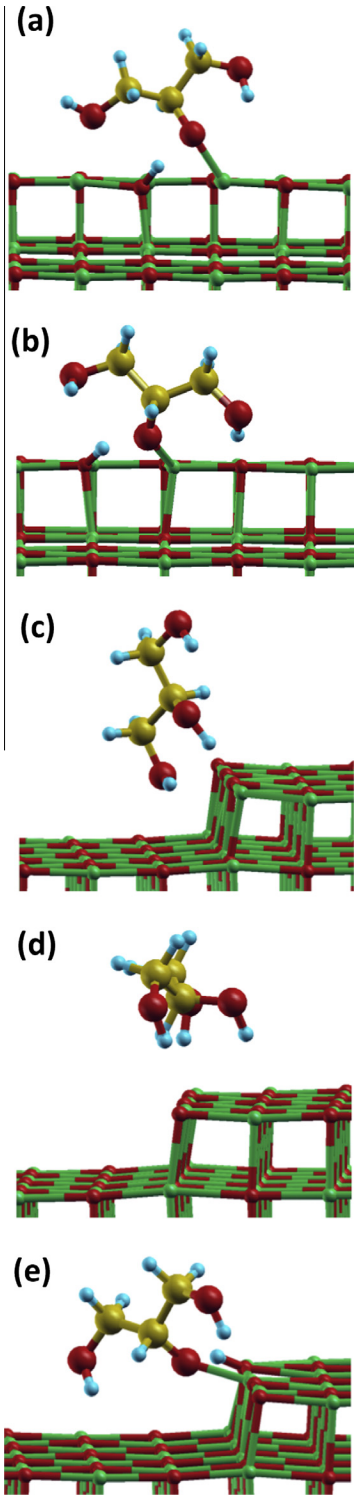

Fig. 8. Optimized geometrical structures of Gly adsorbed on stepped MgO. (a) dissociative adsorption, mode 1OH(2); (b) dissociative adsorption, mode 2OH(1,2); (c) non-dissociative adsorption, mode 2OH(2,3); (d) non-dissociative adsorption, mode $3OH_a$; (e) dissociative adsorption, mode $3OH_b$. Red, green, cyan, and yellow balls are O, Mg, H, and C atoms, respectively. (For the interpretation of the references to color in this figure legend, the reader is referred to the Web version of this article.)

Table 1
Adsorption energy (E_{ads}) and bond distances (d) found to the adsorption of Gly on the stepped MgO surface.

Entry	Mode, nOH(m)	n	m	E_{ads} (eV)	$d_{(H-Os)}$ (Å)	$d_{(O-Mgs)}$ (Å)	$d_{(O-H)}$ (Å)
1 (Fig. 8a)	1OH(2)	1	2	−1.57	1.02	2.01	1.54
2 (Fig. 8b)	2OH(1,2)	2	1, 2	−1.59	1.03	1.91	1.56
3 (Fig. 8c)	2OH(2,3)	2	2, 3	−1.33	1.43	2.14	1.09
4 (Fig. 8d)	$3OH_a$	3	1, 2, 3	−0.53	1.62	3.09	0.99
5 (Fig. 8e)	$3OH_b$	3	1, 2, 3	−1.82	1.00	1.92	1.84

on stepped MgO, these authors observed that in the most preferred situations, the complete deprotonation of Gly takes place [36,37].

Similar to the calculations with the Gly molecule, the molecular modeling of isolated and adsorbed FAME was carried out. The FAME molecule used in the catalytic experiments was methyl oleate, the methyl ester derived from oleic acid in which the long tail contains eighteen carbon atoms and one unsaturation (C18:1). However, for modeling purposes, a shorter saturated methyl ester containing three carbon atoms in the acyl group was used (C3:0).

The calculated intramolecular distances of FAME as an isolated molecule are: $d_{(C=O)} = 1.22$ Å, $d_{(O-CH_3)} = 1.43$ Å, $d_{(C-OCH_3)} = 1.43$ Å), $d_{(C-C)} \approx 1.52$ Å, and $d_{(C-H)} \approx 1.10$ Å.

Optimized structures of FAME adsorbed on a stepped MgO surface are shown in Fig. 9, and the results are summarized in Table 2. From different initial geometries, four adsorption modes were obtained: two with the FAME molecule adsorbed perpendicular to the step direction, and other two situations adsorbed along the edge. In all the situations, FAME adsorbs non-dissociatively. In cases with FAME adsorbed perpendicular to the edge, the interactions through the C=O group (labeled as $FAME_{C=O}$, Fig. 9a) and through the O of the methoxy fragment (labeled as $FAME_O$, Fig. 9b) were found. On the other hand, when FAME was adsorbed along the edge, in one of the situations, the FAME molecule is oriented "standing" over the step (with the O—C=O plane perpendicular to the (100) surface, indicated as $FAME_{stand}$, Fig. 9c); in the other configuration, the molecule is tilted onto the terrace ($FAME_{tilt}$, Fig. 9d). Among all the situations, the most stable adsorption mode resulted to be $FAME_{C=O}$, in which the Mg_s—O distance presents the lowest value ($d_{(O_{C=O}-Mg_s)} = 2.08$ Å), with slight changes in the FAME internal geometry with respect to the free molecule. By examining the net atomic charges, we have observed that when FAME in this configuration interacts with the step Mg^{2+}_{4c} site, polarization of the C=O group (as depicted in Scheme 2) does not proceed to a high extent in comparison with isolated FAME.

By comparing the E_{ads} values of Tables 1 and 2, we conclude that, as in our previous work [8], Gly is more strongly adsorbed than FAME.

3.4.2. FAME adsorption on MgO after β-glyceroxide formation

Once the Gly and FAME adsorptions were independently studied, we modeled both species adsorbed side by side on the step in order to study the glycerolysis reaction. For this reason, we now consider the consecutive adsorption of FAME on the stepped MgO surface, with Gly previously adsorbed as the highly stable β-GlyOx species ($3OH_b$ geometry, Fig. 8e and Table 1, entry 5). Two different types of arrays were considered depending on the desired product: α-MG or β-MG. We found two stable situations in which either the primary or the secondary OH groups of β-GlyOx interact with the carbonyl carbon of FAME. The optimized structures are schematized in Figs. 10a and 11a, respectively. For α-MG formation, the FAME molecule was oriented perpendicular to the stepped surface, such as the $FAME_{C=O}$ geometry, with the carbonyl group close to one primary OH group of β-GlyOx, Fig. 10a; while for the β-MG formation, FAME was oriented lying and parallel to the MgO step, such as the $FAME_{tilt}$ geometry, with the C=O group near to the secondary oxygen of β-GlyOx, Fig. 11a. In the first

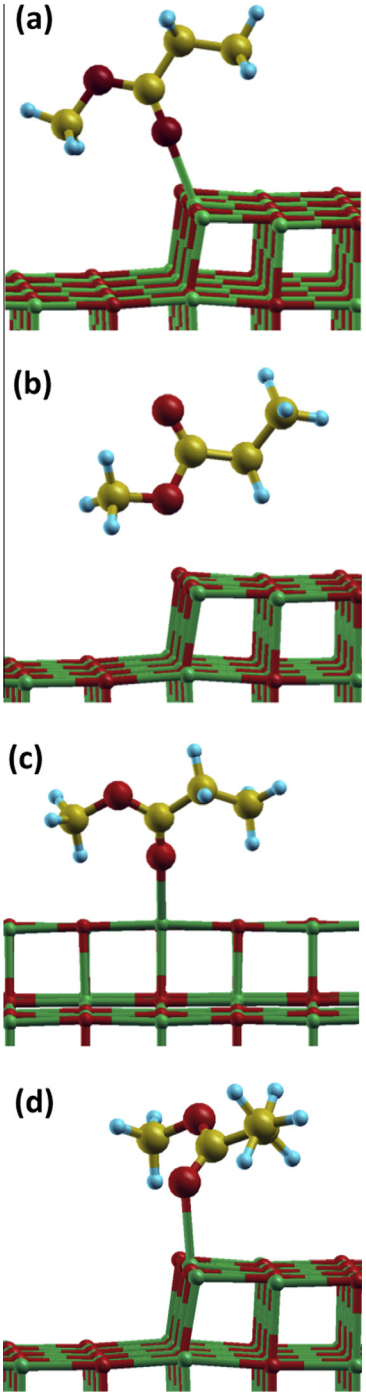

Fig. 9. Optimized structures of FAME adsorbed on stepped MgO. (a) Mode $FAME_{C=O}$; (b) mode $FAME_O$; (c) mode $FAME_{stand}$; and (d) mode $FAME_{tilt}$.

Table 2
Adsorption energy (E_{ads}) and bond distances (d) found to the adsorption of FAME on the stepped MgO surface.

Entry	Mode	E_{ads} (eV)	$d_{(O_{C=O}-Mg_s)}$ (Å)	$d_{(C=O)}$ (Å)
1 (Fig. 9a)	$FAME_{C=O}$	−0.49	2.08	1.23
2 (Fig. 9b)	$FAME_{O}$	−0.28	4.52	1.22
3 (Fig. 9c)	$FAME_{stand}$	−0.29	2.11	1.23
4 (Fig. 9d)	$FAME_{tilt}$	−0.41	2.15	1.24

situation, an optimized distance of 2.98 Å was obtained between the carbon atom of the C=O group of FAME and the oxygen atom of primary OH of β-GlyOx species. In the second array, owing mainly to steric effects, the distance between the carbon atom of the C=O group of FAME and the oxygen atom of the secondary OH of β-GlyOx is much longer (4.15 Å). The optimized paired β-GlyOx/$FAME_{C=O}$ and β-GlyOx/$FAME_{tilt}$ structures were labeled as A_α and A_β geometries, respectively.

The A_α geometry (Fig. 10a) which finally leads to α-MG is calculated to be 0.31 eV more stable than the one that leads to β-MG (A_β geometry, Fig. 11a). Taking into account that the main difference between both geometries is the FAME orientation, we calculated the energy of the FAME adsorption coming from the gas phase, on the stepped MgO surface containing preadsorbed Gly ($3OH_b$ geometry). For FAME in the A_α and A_β geometries, the values are −0.59 and −0.28 eV, respectively. It is interesting to note that the FAME adsorption over MgO containing the β-GlyOx species is in the first case 0.10 eV more stable than onto pure stepped MgO (adsorbed as an isolated molecule at the $FAME_{C=O}$ mode, Table 2, entry 1). This behavior indicates that the pair β-GlyOx/$FAME_{C=O}$ formation which ultimately yields to α-MG is energetically favored.

3.4.3. Reaction mechanisms of FAME glycerolysis

The above-mentioned A_α and A_β geometries were used as starting points to study the reaction paths to form the α-MG and β-MG products, respectively (Figs. 10 and 11). The reaction profiles for both reactions are shown in Fig. 12. In this scheme, the above-defined reaction energy (E_{reac}) is expressed relative to the energy of the Gly, FAME, and MgO as isolated species.

We first studied the complete reaction sequence for the α-MG formation. Optimized geometries of all the involved species are presented in Fig. 10. The reaction occurs through two successive steps: the formation of a tetrahedral intermediate (TI_α), and the final desorption of the products, α-MG and CH_3OH. A tetrahedral intermediate species was also observed by de Lima et al. [38], when the homogeneous transesterification reaction between Gly and methoxide and ethoxide anions was theoretically evaluated. The formation of TI_α takes place by the dissociation of a primary OH group of the adsorbed β-GlyOx and the creation of a new

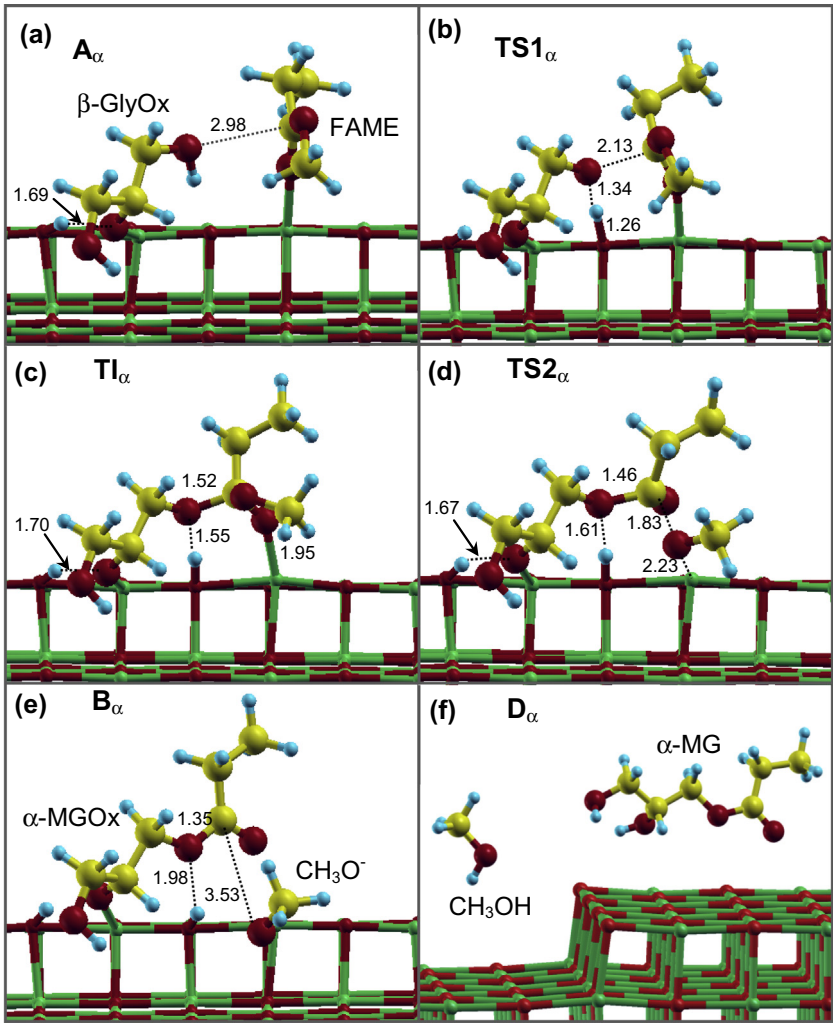

Fig. 10. Optimized structures of the species involved in the FAME glycerolysis reaction to form α-MG. (a) β-GlyOx–FAME coadsorption; (b) transition state 1 ($TS1_\alpha$); (c) tetrahedral intermediate (TI_α); (d) transition state 2 ($TS2_\alpha$); (e) α-MGOx and CH_3O^-; and (f) gas phase α-MG and CH_3OH. Bond distances in Å.

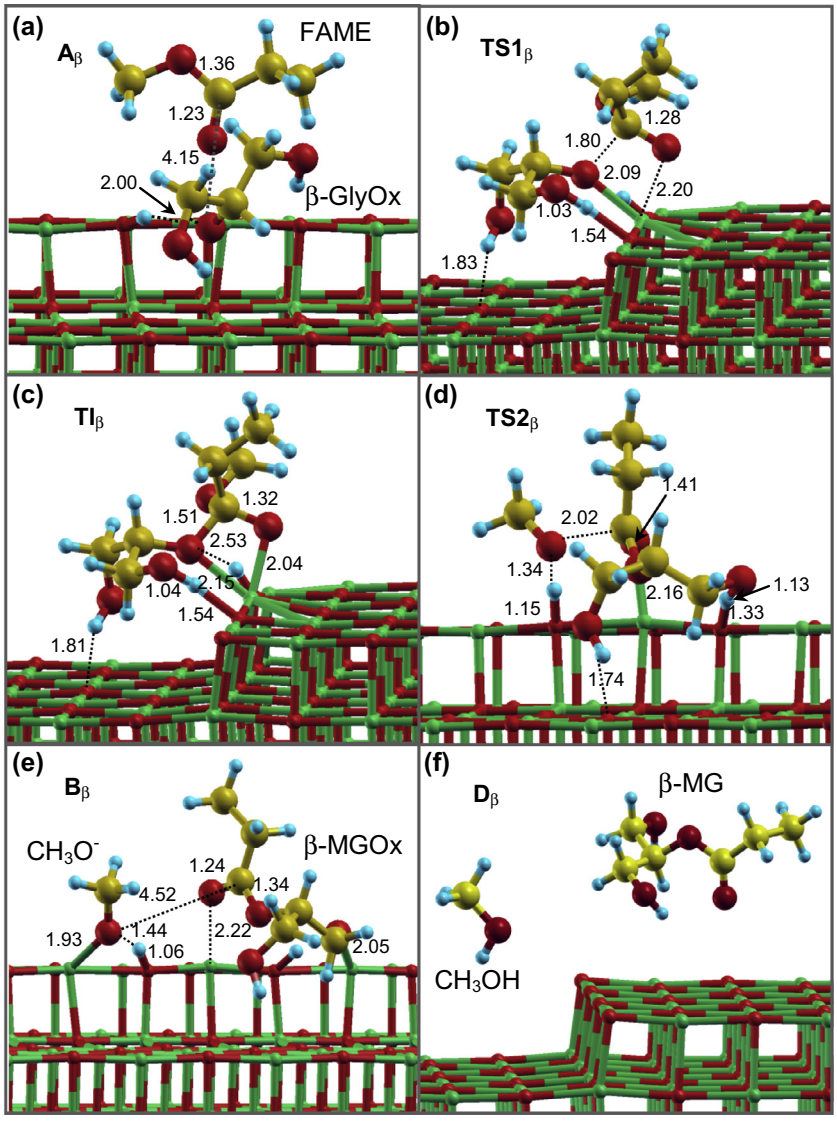

Fig. 11. Optimized structures of the species involved in the FAME glycerolysis reaction to form β-MG. (a) β-GlyOx–FAME coadsorption; (b) transition state 1 ($TS1_\beta$); (c) tetrahedral intermediate (TI_β); (d) transition state 2 ($TS2_\beta$); (e) β-MGOx and CH_3O^-; and (f) gas phase β-MG and CH_3OH. Bond distances in Å.

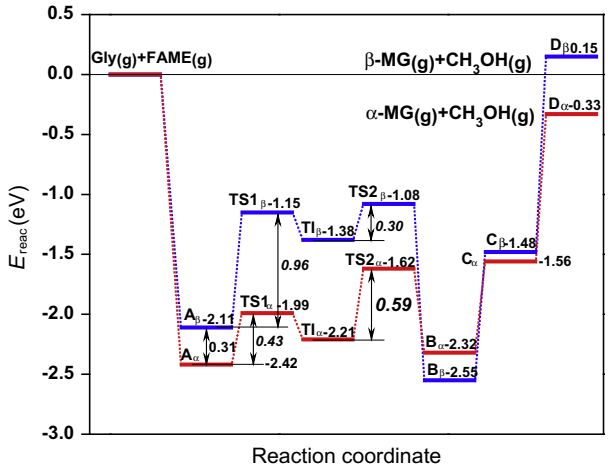

Fig. 12. Reaction energy profile for FAME glycerolysis toward α-MG and β-MG formation.

C—O bond (Fig. 10c). TI_α is strongly connected with the surface by means of two O—Mg_s bonds, one by the O atom formerly belonging to β-GlyOx and other by the C=O group of the FAME fragment. Our results indicate that TI_α is formed from the initial configuration by crossing an energetic barrier of 0.43 eV, corresponding to the first transition state ($TS1_\alpha$, Fig. 10b). The geometry of the activated complex involves the stretching of the O—H bond belonging to the primary hydroxyl group, the approach of the carbonylic C atom, and the reorientation of the hydrocarbon chain. The relative strong hydrogen bonds between the O of the formerly primary hydroxyl of Gly fragment with the resulting surface OH at both $TS1_\alpha$ and TI_α species help stabilize these structures.

The second reaction step, indicated as B_α geometry in Fig. 10e, comprises the α-monoglyceroxide species (α-MGOx) formation and the releasing of CH_3O^-; the latter ends linked to the edge through a O—Mg_s bond of 1.99 Å. The finally formed C—O bond which connects the acyl group with the rest of the ester molecule results in a distance of 1.35 Å. The transition state associated with this step ($TS2_\alpha$, Fig. 10d) requires higher energy (0.59 eV) than the first one (0.43 eV). This reaction step is slightly exothermic (−0.11 eV). The activated complex geometry involves the separa-

tion of the methoxide group and its simultaneous approach to an edge Mg^{2+}_{4c} cation. To complete the reaction, α-MG and methanol molecules must be formed as adsorbed species from α-MGOx and CH_3O^-, respectively. This stage of the reaction involves the formation of two new O—H bonds: one at the α-MG molecule (secondary OH group of the Gly fragment) and the other belonging to methanol. The required energy on this step is 0.76 eV (Fig. 12, evolution between B_α and C_α geometries). The subsequent desorption of both molecules needs again of additional energy (Fig. 12, evolution between C_α and D_α geometries). In Fig. 12, the energy of the D_α geometry (pictured in Fig. 10f) corresponds to the total energy of the separated fragments, i.e., α-MG, methanol, and bare MgO.

Let us now consider the formation of β-MG. The corresponding optimized geometries of all the species are shown in Fig. 11. As it was previously mentioned, the FAME molecule is far away from the secondary OH group of β-GlyOx. In this structure (A_β geometry), both molecules are sharing the same Mg^{2+}_{4c} cation at the stepped MgO surface (Fig. 11a).

The first step of this reaction consists also in the formation of the tetrahedral intermediate, TI_β, through the activated complex $TS1_\beta$ (Fig. 11b). In $TS1_\beta$, the new formed C—O bond is at 1.80 Å. Besides, the Mg^{2+}_{4c} at the edge is significantly puckered up. Two hydrogen bonds between both primary OH groups and the oxide surface are present in this activated complex (with oxygen anions at edge and terrace); despite of that, the required energy to form TI_β (0.96 eV) is more than twice the one needed to form TI_α (0.43 eV). The tetrahedral intermediate TI_β is sterically hindered (Fig. 11c), because the new C—O bond connects two bulky chains at very short distance (1.51 Å). As is clear from Fig. 11c, this configuration is highly unstable in comparison with TI_α (Fig. 10c).

The second reaction step, that comprises the β-monoglyceroxide (β-MGOx) formation and the release of CH_3O^-, geometry B_β (Fig. 11e) is highly exothermic (−1.17 eV). In $TS2_\beta$ geometry, the outgoing methoxide group is stabilized by a strong hydrogen bond with the surface OH formed during the initial chemisorption (Fig. 11d). The new C—O bond at TI_β is reduced to 1.41 Å, and the O atom belonging to C=O maintains the link with the surface but more enlarged (2.16 Å). Due to steric effects, $TS2_\beta$ is highly unstable and the TI_β transforms into β-MGOx and CH_3O^- surpassing a low barrier (0.30 eV). Such a structure was called B_β geometry (Fig. 11e), in which β-MGOx is bonded to the surface mainly through one primary OH group of the Gly fragment, whereas the methoxide species results doubly bonded to Mg^{2+}_{4c} and OH. Notice that the C=O group practically loses its interaction with the Mg^{2+}_{4c} located at the edge of the surface. For the final formation of β-MG and methanol molecules, the energetic requirement is 1.07 eV (evolution between B_β and C_β geometries, Fig. 12), a value higher than that for the α-MG/methanol adsorbed pair (0.76 eV). In addition, the last step, D_β geometry (Fig. 11f), that comprises the release of β-MG and methanol species to the gas phase, demands the highest energy cost of the whole process.

Finally, we have performed complementary calculations to test possible FAME solvent effects. Since the reaction takes place in a dilute solution of Gly in FAME, we have measured the influence of other FAME molecules in one particular path, namely, the first step of reaction to produce α-MG (Fig. 10a–c). For that, we have explicitly added three FAME molecules surrounding the β-GlyOx/FAME pair (A_α geometry). Taking into account the large size of FAME molecules, three seems to be a sufficient number to evaluate short-range effects due to the solvent. The results showed a stabilization value of about 0.4 eV in the reaction energies (measured with respect to the isolated fragments) of all the species involved in this step: A_α, TS1, and TI_α. However, the difference among the species is essentially the same: the reaction energy difference between A_α and TI_α is 0.20 eV with additional FAME molecules and 0.21 eV without them (Fig. 12). Besides, the activation energy from A_α to TI_α is calculated to be 0.41 eV with explicit solvation, and 0.43 eV without it. Regarding the geometries, the most affected distance is the C—O bond between β-GlyOx and FAME fragments (A_α geometry, Fig. 10a) which is slightly shortened by 0.05 Å with solvation. The O—H distance of the primary hydroxyl of β-GlyOx does not change along the reaction step. The other distances are altered by 0.03 Å at most. Therefore, the solvent seems to stabilize all the species in a similar manner in such a way that the energy differences are affected only slightly.

4. Conclusions

The catalytic results showed that the MgO active site for the glycerolysis reaction is a strongly basic oxygen anion, i.e., a coordinatively unsaturated oxygen located on corners or edges of the MgO surface. In the catalytic tests, the main monoglyceride isomer was always the α-glyceryl monooleate (α-MG) whereas the diglyceride isomer was the 1,3-glyceryl dioleate (1,3-DG).

The glyceride products form by C—O coupling of FAME with glycerol at one of the glycerol OH groups. The preferential formation of glycerides containing the ester fragment at positions 1 and/or 3 of the glycerol molecule could not be extensively modified by changing the reaction temperature or reactant ratio in a wide range.

In agreement with the catalytic results, the calculations presented here predict that α-MG formation is favored over that of β-MG, in spite of the fact that the glycerol secondary O—H bond cleavage is energetically favored. These results are explained by the theoretical modeling by considering that:

(i) Gly adsorption occurs preferentially through the dissociation of its secondary OH group on the unsaturated basic sites at the edge of a stepped MgO surface. This initial step is barrierless, and a β-glyceroxide species is formed.
(ii) The β-glyceroxide species participates in formation of both, α-MG and β-MG.
(iii) The interaction of β-glyceroxide with FAME occurs more favorably through one of the two remaining primary OH groups of the β-glyceroxide species because the secondary O atom is more sterically hindered and hence, less available to react. For this reason, a primary OH group of glycerol finally participates in the C—O bond formation giving preferentially α-MG instead of β-MG.
(iv) The tetrahedral intermediate TI_α leading to α-MG is relatively easy to form due to its relaxed geometry, which allows a strong interaction with the surface.
(v) The limiting step of the pathway to β-MG is clearly the formation of the tetrahedral intermediate TI_β, owing to large sterical effects. In fact, once this intermediate disappears, the energy abruptly falls down.

Acknowledgments

Authors thank Universidad Nacional del Sur (UNS), Universidad Nacional del Litoral (UNL), Consejo Nacional de Investigaciones Científicas y Técnicas (CONICET) and Agencia Nacional de Promoción Científica y Tecnológica (ANPCyT) of Argentina, for the financial support of this work.

References

[1] A. Corma, S. Iborra, A. Velty, Chem. Rev. 107 (2007) 2411–2502.
[2] J.W. Shabaker, G.W. Huber, J.A. Dumesic, J. Catal. 222 (2004) 180–191.
[3] A. Corma, G.W. Huber, L. Sauvanaud, P. O'Connor, J. Catal. 247 (2007) 307–327.
[4] R.S. Karinen, A.O.I. Krause, Appl. Catal. A: Gen. 306 (2006) 128–133.
[5] Y. Zheng, X. Chen, Y. Shen, Chem. Rev. 108 (2008) 5253–5277.

[6] F. Jerome, Y. Pouilloux, J. Barrault, ChemSusChem 1 (2008) 586–616.
[7] A. Corma, S.B.A. Hamid, S. Iborra, A. Velty, J. Catal. 234 (2005) 340–347.
[8] C.A. Ferretti, S. Fuente, R. Ferullo, N. Castellani, C.R. Apesteguía, J.I. Di Cosimo, Appl. Catal. A: Gen. 413–414 (2012) 322–331.
[9] J.I. Di Cosimo, V.K. Díez, C.R. Apesteguía, Appl. Catal. A: Gen. 137 (1996) 149–166.
[10] C.A. Ferretti, R.N. Olcese, C.R. Apesteguía, J.I. Di Cosimo, Ing. Eng. Chem. Res. 48 (2009) 10387–10394.
[11] C.A. Ferretti, C.R. Apesteguía, J.I. Di Cosimo, J. Argentine Chem. Soc. 98 (2011) 16–28.
[12] G. Kresse, J. Hafner, Phys. Rev. B 47 (1993) 558–561.
[13] G. Kresse, J. Hafner, Phys. Rev. B 48 (1993) 13115–13118.
[14] G. Kresse, J. Hafner, Phys. Rev. B 49 (1994) 14251–14268.
[15] P. Blochl, Phys. Rev. B 50 (1994) 17953–17979.
[16] G. Kresse, D. Joubert, Phys. Rev. B 59 (1999) 1758–1775.
[17] J.P. Perdew, K. Burke, M. Ernzerhof, Phys. Rev. Lett. 77 (1996) 3865–3868.
[18] H.J. Monkhorst, J.D. Pack, Phys. Rev. B 13 (1976) 5188–5192.
[19] M. Methfessel, A.T. Paxton, Phys. Rev. B 40 (1989) 3616–3621.
[20] P. Broqvist, H. Grönbeck, I. Panas, Surf. Sci. 554 (2004) 262–271.
[21] N.V. Skorodumova, K. Hermansson, B. Johansson, Phys. Rev. B 72 (2005) 125414.
[22] C. Chizallet, G. Costentin, M. Che, F. Delbecq, P. Sautet, J. Phys. Chem. B 110 (2006) 15878–15886.
[23] J.I. Di Cosimo, V.K. Díez, C. Ferretti, C.R. Apesteguía, Catalysis 26 (2014) 1–28.
[24] J.I. Di Cosimo, V.K. Díez, M. Xu, E. Iglesia, C.R. Apesteguía, J. Catal. 178 (1998) 499–510.
[25] R. Philipp, K. Fujimoto, J. Phys. Chem. 96 (1992) 9035–9038.
[26] C. Morterra, G. Ghiotti, F. Boccuzzi, S. Coluccia, J. Catal. 51 (1978) 299–313.
[27] T. Kimmel, Kinetic Investigation of the Base-catalyzed Glycerolysis of Fatty Acid Methyl Esters, PhD Thesis, Institut fur Chemie, TU, Berlín, Germany, 2004.
[28] A.E. Andreatta, L.M. Casás, P. Hegel, S.B. Bottini, E.A. Brignole, Ind. Eng. Chem. Res. 47 (2008) 5157–5164.
[29] J. Barrault, Y. Pouillox, J. Clacens, C. Vanhove, S. Bancquart, Catal. Today 75 (2002) 177–181.
[30] G.F. Froment, K.B. Bischoff, Chemical Reactor Analysis and Design, second ed., John Wiley and Sons, New York, 1990. p. 176.
[31] C.A. Ferretti, A. Soldano, C.R. Apesteguía, J.I. Di Cosimo, Chem. Eng. J. 161 (2010) 346–354.
[32] J.I. Di Cosimo, A. Acosta, C.R. Apesteguía, J. Mol. Catal. A: Chem. 234 (2005) 111–120.
[33] J.K. Bartley, C. Xu, R. Lloyd, D.I. Enache, D.W. Knight, G.J. Hutchings, Appl. Catal. B: Environ. 128 (2012) 31–38.
[34] H. Adkins, F.W. Cox, J. Am. Chem Soc. 60 (1938) 1151–1159.
[35] C.F. de Graauw, J.A. Peters, H. van Bekkum, J. Huskens, Synthesis (1994) 1007–1017.
[36] M. Calatayud, A.M. Ruppert, B.M. Weckhuysenfor, Chem. Eur. J. 15 (2009) 10864–10870.
[37] M. Calatayud, Catal. Today 152 (2010) 88–92.
[38] E.F. de Lima, J.W.deM. Carneiro, C. Fenollar-Ferrer, S. Miertus, S. Zinoviev, N.C. Om Tapanes, D.A.G. Aranda, Fuel 89 (2010) 685–690.